Title: Charge Density Analysis Attending Bond Torsion: A Bond Bundle Case Study

Authors: Jordan Goss, Tim Wilson, Amanda Morgenstern, Mark Eberhart

Abstract:

For nearly a century chemical understanding has been tied to the properties of bonds, though more often than not, these bond properties are rooted in molecular orbital or valence bond representations of the electronic structure. Technological advances, however, are allowing for experimental measurements of the density via high resolution x-ray diffraction, while theoretical insights are opening the door to its direct calculation using fast and potentially versatile orbital free DFT methods. Capitalizing on these emerging tools without sacrificing hard won orbital derived understanding has spurred a search for density based representations that deliver the same information available from the orbital perspective. We show that recent extensions of the QTAIM formalism are useful as a means of recovering some of the bond properties that have become an intrinsic part of our chemical understanding. Specifically, we compute from the density the changing bond order accompanying the rotation about a double bond using the well-studied fulvene molecule as a test case. We compare the picture that emerges from this density based perspective with that stemming from molecular orbital approaches and argue that the two viewpoints are compatible.

Introduction:

Valence bond and molecular orbital theories are the most common formalisms used to visualize and predict the redistribution of electrons accompanying atomic movement. These approaches complement one another by providing different vantage points from which to view an inherently complex and only partially understood phenomenon. However, advances in the techniques of high resolution x-ray diffraction over the last quarter century have made it possible to image the charge density and spawned a new discipline of charge density analysis (1), which, by default, seeks to rationalize chemical properties from an orbital free perspective. If we are to build a consistent theory for the structure and redistribution of charge, we must develop density based representations of familiar orbital properties. We have found the quantum theory of atoms in molecules (QTAIM) (2) and its recent extensions (3-6) provides an approach toward achieving this objective.

QTAIM methodologies are motivated by the desire to associate molecular properties with the structure of the charge density, $\rho(r)$. As such, these methods are consistent with the foundational principles of density functional theory (DFT), lend themselves to easy visualization, and can be applied to any system in which $\rho(r)$ is known to some arbitrary accuracy, for example, as determined via band methods, real space orbital based methods, orbital free approaches, or experimentally determined densities.

One of the first QTAIM efforts to describe the evolution of $\rho(r)$ resulting from atomic motion

originated with Bader's applications of catastrophe theory to elucidate the topological constraints to charge redistribution (2). From this perspective, it is not the movement of individual electrons that is of concern, but rather the movement of charge density critical points (CPs)—maxima, minima, and saddle points.

With CPs replacing electrons as the focus of attention in the QTAIM approach, Ayers et al. proposed an electron preceding perspective (EPP) (7), which predicts that CP movement occurs most readily along directions where charge density is flattest. Jenkins et al. expanded on the EPP through an investigation of the exemplary fulvene system (8). In particular, Jenkins focused on the changes to and about the CP characteristic of fulvene's exo-double bond as it underwent a 90° rotation. The substantial barrier to rotation about this bond is known to decrease for the excited state (8). From an EPP perspective this observation suggests that the excited state density is flatter than the ground state density, which Jenkins et al. demonstrated to be the case.

An interesting aspect of this work was the assessment of the C-C bond evolution from double to single character as a result of the rotation. This assessment used density related arguments based on the ellipticity of $\rho(r)$ at the CP characteristic of the rotated bond. Here we expand on the QTAIM approach by employing extensions to the theory that are able to recover a richer representation of charge density evolution. We demonstrate that these extensions illuminate the changing character of the bond accompanying the rotation via a direct determination of bond order and also through an intuitive 3-D visualization.

Background

QTAIM has proven useful as a way to associate molecular and solid state properties with the structure of $\rho(r)$, where structure is characterized in terms of topological and geometric properties (2, 9–11). In turn, and quite generally, the topology of $\rho(r)$ can be categorized by way of the elements of its relative critical sets (RCSs), which are defined according to the orthogonality between the three eigenvectors (ε_i, i ∈ {1, 2, 3}) of the Hessian of charge density (Hρ) and its gradient ($\nabla\rho$) (10).

Elements of the 0-, 1-, and 2-dimensional RCSs are respectively the sets of points where three, two, or one of the eigenvalues of Hρ are orthogonal to $\nabla\rho$, i.e., where $\nabla\rho(r)\cdot\varepsilon_i = 0$. Elements of the 0-D RCS are the points where $\nabla\rho$ vanishes, and as such, are the critical points (CPs) of Morse Theory (13)—maxima, minima, and saddle points of index +1 and -1. Elements of the 1-D RCS are distinct gradient paths (GPs), which must originate and terminate at CPs. Elements of the 2-D RCS are distinct gradient surfaces that are necessarily bounded by elements of the 1-D RCS.

QTAIM formalism (2) associates chemical structure with elements of the RCS. For example, charge density maxima are coincident with nuclei and hence are called nuclear-CPs (nCPs). An element of the 1-D critical set connecting two nCPs is called a bond path and must pass through

a -1 saddle point called a bond-CP (bCP). Of particular significance to the QTAIM formalism are the unique volumes bounded by gradient surfaces (zero-flux in the gradient of the charge density) and consequently have well-defined and additive energies, which is not true of arbitrary volumes (11). Every molecule and solid may be uniquely partitioned into space filling volumes containing a single nCP and bounded by elements of the 2-D RCS, which are designated as atomic basins or Bader atoms. In addition, atomic systems may also be uniquely partitioned into space filling volumes bounded by elements of the 2-D RCS containing a single bCP and bond path. These volumes are designated bond bundles (BBs) (3,4).
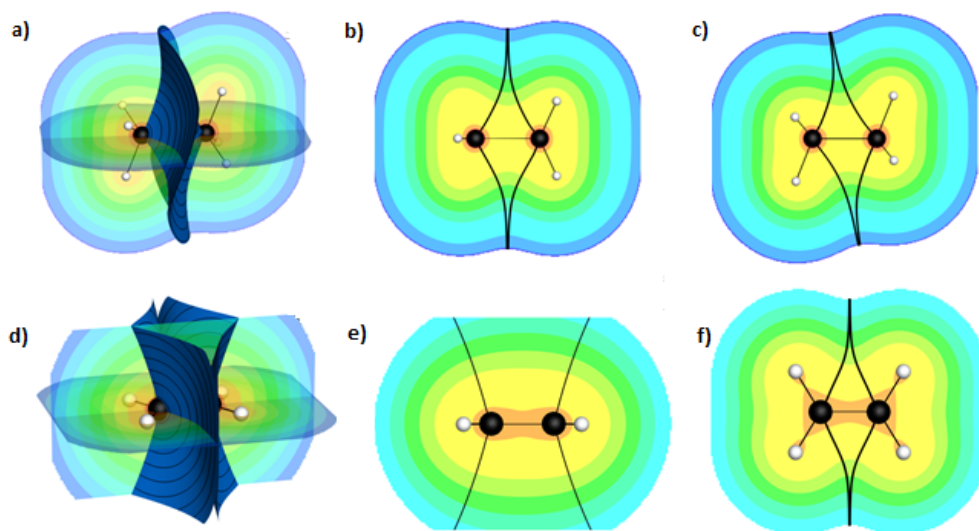

Figure 1: (a-c): The surfaces of the C-C bond bundle of ethane and two perpendicular cut planes containing the C-C axis. The BB converges in all directions as can be seen by the intersection of the bond bundle with the xz (b) and yz (c) cut plane. (d-f): The surfaces of the C-C bond bundle of ethane and two cut planes. The surfaces of this bond bundle are diverging perpendicular to the xz plane shown (e), and converging in the plane of the molecule (f). The bond bundle of ethene is said to be open normal to the molecular plane and closed in the plane.

BBs have characteristic shapes that have been argued to mediate chemical reactivity (14), and can be described generally as open or closed. For example, as shown in Figure 1, the BB in ethane is defined as closed because its faces are asymptotically converging. On the other hand, for ethene the BB is defined as open in one direction, with diverging faces perpendicular to the molecular plane, but closed parallel to the plane.

As volumes, BBs can be used to make contact with the concept of bond order (BO) (10) as half the number of valence electrons it contains. BB bond order can be determined using only the total charge density by assuming a radial distribution of core electrons as demonstrated in (10). In practice, this number can equivalently be determined from an electronic structure calculation by integrating the valence electron density of the BB out to an arbitrarily distant cutoff surface,

typically chosen as the 0.001 electron/bohr^3 isosurface (2,15). Using this integration scheme, the ethane C-C bond order is 0.91 and the bond order of ethene is 1.72.

Methods:

Our objective for this investigation is to follow the progression of BBs through a chemically important process and compare the picture that emerges with that derived from orbital perspectives. Rotation about a C-C double bond is a central and pervasive chemical process, which is represented by multifaceted orbital models. Hence, we chose to investigate BB evolution associated with the rotation around a C-C double bond and in particular the exo-double bond of fulvene (Figure 2), which, as has been mentioned, is an exemplar system for investigations of bond torsion.
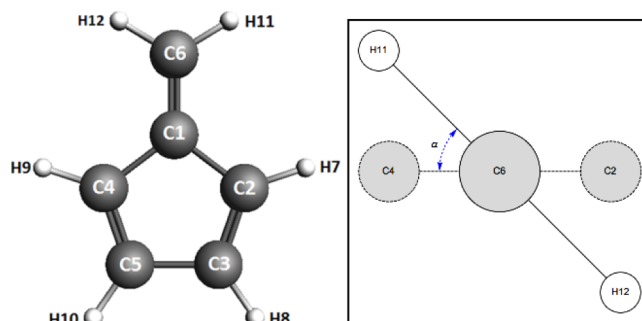

Figure 2: Fulvene molecule (left) with carbon (C1-C6) and hydrogen (H7-H12) atoms labeled. The rotation of the methyl group about the C1-C6 bond axis is depicted on the right. The methyl group is rotated in α=10° increments from planar to the ring (0°) to perpendicular to the ring (90°).

Of particular note is the study of Jenkins et al., who, working at the CASSFC/cc-pvdz level of theory with an active space of six electrons in six orbitals (8, 16–18), identified atomic coordinates for structures on the ground state potential energy surface for rotations of 0°, 63° and 90° degrees, which we refer to respectively as S_0, S_{63} and S_{90}. Of significance was the finding that S_{63} and S_{90} lie along the seam of a conical intersection between the ground and excited state.

We used molecular-orbital DFT methods to calculate the electronic structure and charge density of a fulvene molecule at nine roughly 10° rotational increments about the C1-C6 bond. Molecular coordinates along the rotation were found through relaxation of a rigid rotation of the methylene group at each rotational interval. The relaxations between 0° and less than 63° were very small, for example the C1-C6 bond length varied between 134 and 135 pm. However, between 63° and less than 90° we found a nearly degenerate set of molecular geometries associated with nearly rigid rotations around a longer C1-C6 bond of approximately 146 pm. (A full list of bond lengths for all calculations is given in Table S2.) For every calculation along the rotation coordinate the total energies, spin orbital (SO) energies, and charge densities were obtained with the Amsterdam Density Functional Package, ADF, version 2016 (19), employing an all-electron relativistic triple ζ singly polarized basis set and the CAMY-B3LYP functional (20). This functional is a range separated hybrid and recovers quality information for the frontier orbitals essential for excited state calculations. Values of the charge density were imported into Tecplot on a 0.049 Å grid size. The Bondalyzer add-on package in Tecplot was used to analyze the BBs and their bond orders (21).

Results:

We analyzed the orbital representation of the charge density with respect to the C_2 point group—the symmetry conserved through the rotation—which admits two one dimensional irreducible representations, **A** and **B**. The state of the rotation is described by the occupancy of the three near Fermi energy orbitals: **9B**, **10B** and **12A** shown in (Figure 3). These spin orbitals (SOs) may be characterized as π–bonding (**9B**) and π–antibonding (**10B**) on the exo-double bond, and π–nonbonding (**12A**) on the exo-double bond as this orbital resides primarily on the ring. The ground state of S_0 was found to have an occupancy for these near Fermi energy orbitals of $\{9B^2\ 12A^2\ 10B^0\}$, which we refer to as the O_1 occupancy. On the other hand, the occupancy of the ground state of S_{90} was found to be $\{9B^1\ 12A^2\ 10B^1\}$, referred to as O_2, which admits both a singlet and triplet configuration. For our calculations, however, the triplet configuration was of slightly lower energy (~ 0.1 eV). Further, the SOs, and density for the two occupancies were, for our purposes, inconsequentially different. Hence all
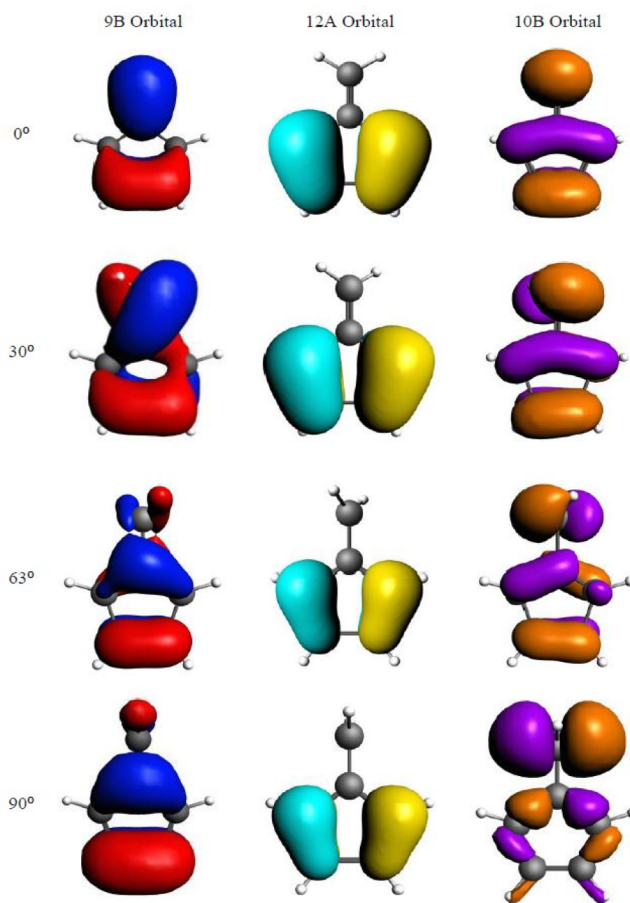

Figure 3: The near fermi energy SOs of the S_{63} coupled by the rotation (see Figure 4). The 9B SO is π-bonding between C1 and C6 while the 10B SO is π -antibonding between the same two atoms.

reference to O_2 indicates the triplet configuration. Finally, for S_{63}—at the root of the conical intersection—the low energy occupancy is the triplet configuration $\{9B^2\ 12A^1\ 10B^1\}$ which we designate as O_3.

Figure 4 depicts the evolution of the SOs at selected points along the rotation. At rotations of less than 63°, O_1 is of lowest energy. Beyond this point O_2 and O_3 are of lower energy. However, which of these two is of lower energy is sensitively dependent on molecular geometry. For the 63° rotation the SO energies result in an aufbau occupation of O_3 and a nonaufbau O_2, while at 70° the
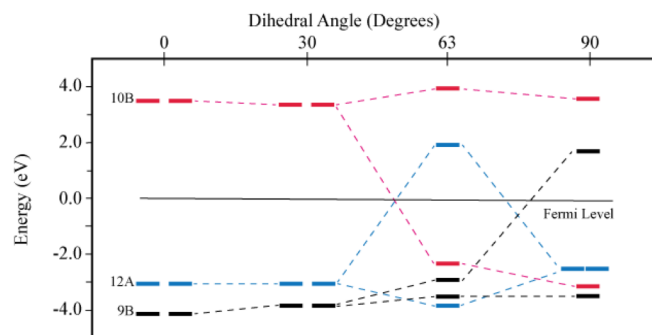
Figure 4: The SO levels diagram for O_1 at 0° and 30°, O_3 at 63°, and O_2 at 90° rotations.

situation is reversed with an aufbau O_2 and nonaufbau O_3. Small change in C-C bond length or the H-C-H bond angle at 63° or 70° may invert aufbau character of O_2 and O_3.

These observations are consistent with previous work (8) indicating that rotations between 63° and 90° lie on the seam of a conical intersection. In such a situation one cannot separate nuclear and electronic coordinates due to vibronic contributions to the energy (22). Hence it is impossible to associate a discrete electronic state with a specific set of nuclear coordinates.
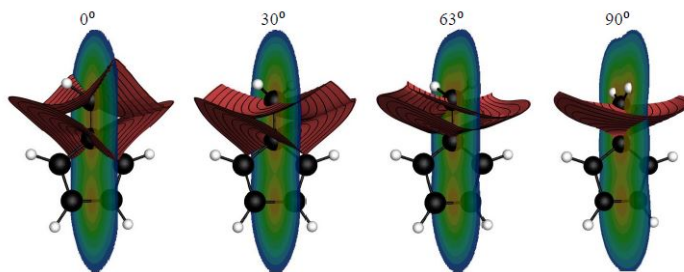

Figure 5: Fulvene C1-C6 bond bundles for O_1 as a function of rotation angle. The BBs for O_2 and O_3 show similar behavior, progressing from the open structure characteristic of ethene to the closed structure characteristic of ethane.

While there is not a unique electronic wave-function along the seam of the intersection, there will be a set of wave-functions that mix to a degree controlled by both the nuclear positions and **momenta**. Accordingly, the electronic charge density will evolve within an envelope of densities corresponding to these individual wave-functions. Our calculations suggest that mixing between wave-functions of O_1, O_2, and O_3 is the primary driver of charge redistribution. Accordingly, we turn now to a discussion of the BB evolution of the states of these principal occupancies.

For all occupations, the rotation driven BB evolution is visually similar to that depicted in Figure 5, where the BBs for O_1 at rotations of 0, 30, 63, and 90 degrees are shown. (Movies that give more detailed 3-D representation of the BB for the selected points are provided in the SI.) Initially all BBs resemble that of the double bond of ethene (Figure 1d-f)—open in the plane perpendicular to the molecular plane—and proceed to fully closed by 90° when they closely resemble the single C-C BB of ethane (Figure 1a-c). While the evolution of the BBs is
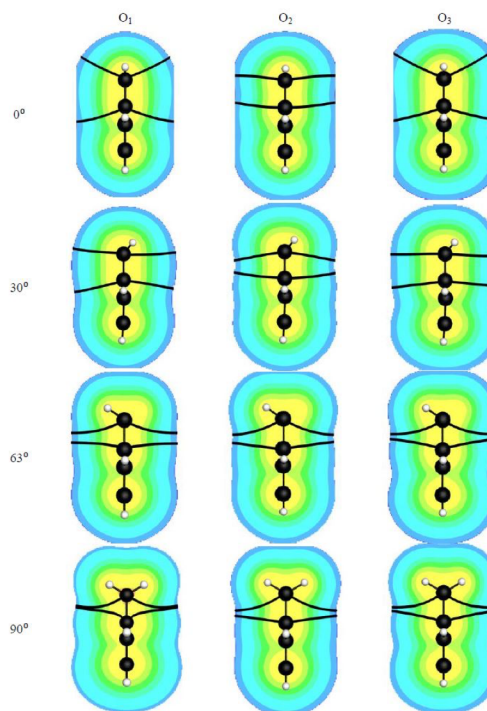

Figure 6: The heavy lines mark the intersection of the BB with the cut plane of Figure 5, permitting a more accurate assessment of BB closure for the three occupancies (columns) as a function of bond rotation (rows). Note the pronounced difference of the BB shapes for the three occupancies.

similar, each has a distinctive shape and closes at a different rate. Figure 6 helps to illustrate this point by depicting the intersection of the BB surfaces with the cut plane of Figure 5. Inspection of this Figure reveals the rotation angles at which the various BBs switches from open to closed in the direction normal to the molecular plane, as gauged by whether the intersection lines are converging or diverging moving away from the C1-C6 bond path. For O_2 the switch from diverging to converging occurs very early in the rotation, in fact the lines appear parallel—marking the switch—for the planar molecule. For O_3 the switch occurs just beyond 30°, while for O_1 it is near 40°.

Using the BB shape as a measure of similarity, the Hammond postulate (23) is easily accessible from the BB perspective. Across all calculation methods—both those performed as a part of this study and those drawn from the literature—the barrier to rotation for all occupations occurs somewhere near 63°. Taking the BBs of the three occupancies of S_{63} as a qualitative representation of the transition state charge density, one may use the "openness" of the 0° BB as a measure of similarity to the transition state. In this manner, O_2 most resembles the transition state and should possess the lowest barrier, as is observed (3). Also, as the transition state BBs more closely resembles the product BBs (90° rotation) than the reactant BB (0° rotation), the transition state should occur late in the rotations, as it does.

A more quantitative picture of BB evolution is provided in Figure 7 where the BB valence electron count (twice the BO) is pictured at each of the 10° rotation increments for all three occupancies. The shaded region corresponds to the points along the conical intersection where the nuclear and electronic wave-functions are inseparable and hence BB electron counts in this region serve only to qualitatively bound the envelope of allowed BOs through the rotation. The BO trend of the C-C bond is consistent with a transition from double to single bond character. Starting with the planar molecule, we calculate a BO of 1.66, 1.46, 1.71 for O_1, O_2, and O_3 respectively, compared to the BO of 1.71 calculated for ethene. (It is unsurprising that O_2 should have the lowest BO as an electron has been moved from a π–bonding to a π–antibonding SO.) After completing the rotation, the calculated BOs for ground state O_2 is 1.24 and for the excited states O_1 and O_3 are 1.82 and 1.24 respectively. All larger than the 0.91 BO of ethane. For all three states, we attribute the comparatively large BO to the occupation of the BB by
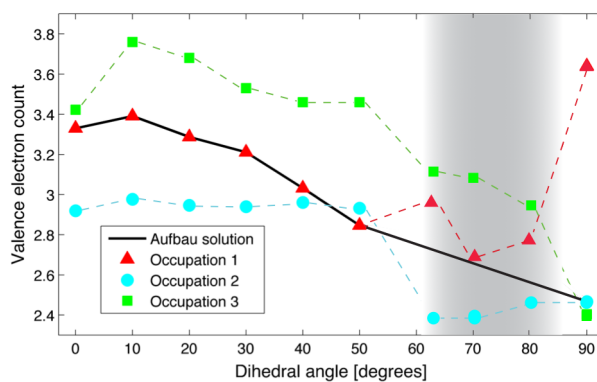

Figure 7: The valence electron count of the C1-C6 bond bundle for the full rotation of the methylene group on fulvene. The shade region corresponds to the points along the conical intersection where the nuclear and electronic wave-functions are inseparable. The black line connects the lowest energy occupancy with SOs occupied in accordance with the aufbau principle.

radical electrons. Intriguingly, even small distortions of H12 and H13 out of the vertical mirror plane produces radical bundles (similar to lone pair bundles observed in other systems (4, 13)) that are separate from the C-C and C-H BBs. Obviously, the electron count in the C1-C6 BB decreases with the formation of these radical bundles. A more detailed study of this phenomenon would require a further decomposition of the charge density into spin-minority and spin-majority BBs, which, though interesting, would be a digression from the focus of this paper.

A further analysis of the calculated BOs is consistent with the spatial distribution of the HOMO and LUMO. For example, consider O_2, where an electron has been promoted from the 9B to the 10B SO of Figure 3. While the 10B orbital may be described as anti-bonding between C1 and C6, it is simultaneously bonding between C1 and C2, between C1 and C4, between C6 and H11, and between C6 and H12; where we describe bonding in the sense of Berlin's (24) binding and anti-binding regions in which, by the electrostatic theorem (25, 26), the electron density acts to either pull nuclei together or separate them. So, while the occupation of the 10B SO will decrease the bond order of the C1-C6 bond, it will concurrently lead to an increase in the bond order of the C-H methylene bonds and the C-C ring bonds, which is observed both visually and quantitatively through BB analysis (see S4). (The C1-C6 bond bundle size decreases through rotation, which is consistent with a loss of electrons, requiring the number of electrons in the C6-H and in the ring to increase.) Hence, BB analysis provides a sensitive probe of electron redistribution between bonds, and can be used to provide a quantitative supplement to electron pushing approaches.

Also, shown in Figure 7, designated by the solid line, are the BB electron counts corresponding to the low energy state for which a Born Oppenheimer solution exists. This line is taken to represent a one-electron characterization of the evolution of the charge density through the rotation and gives rise to a generally decreasing electron count and corresponding BO.

Conclusion:

We demonstrated that bond bundles are an intuitive and accurate tool for describing the evolution of the entirety of the charge density associated with molecular motion in general and the rotation about a C-C double bond in particular. The BB approach provides a representation of rotation about a π-bond that is remarkably consistent with that from orbital approaches. The BB shows a continuous change from open to closed consistent with a transformation from double to single bond character. The rate of closing appears to be related to the barrier to rotation, where the BB of the state with the lowest barrier to rotation closes fastest. In addition, the bond order, as determined from the integration of BB valence density, decreases from 1.66 to 1.24 through the rotation, with the charge density lost from the C-C bond displaced to the methylene C-H bonds and the C ring structure. In all ways, the behavior of the BB transitioning from double to single bond complements conventional views of rotation of a π-bond, but is free from orbital representations and may be particularly useful for quantifying and rationalizing charge redistribution where orbital information is not available, such as from experimentally determined

charge densities, or the calculated charge densities of extended systems where orbital interpretations are difficult. We wish to emphasize that BB decomposition and following is but a tool for the analysis of charge density. Obviously, the more precise the charge density—obtained by whatever means—the more accurate will be any interpretations of charge redistribution that flow from BB analysis.

Conflicts of Interest
There are no conflicts of interest to declare.

References:

1.   Modern Charge Density Analysis, Springer Dordrecht Heidelberg London New York, Editors Gatti C., Macchi P. (2012).

2.   Bader RFW. Atoms in Molecules, a Quantum Theory. Oxford, UK: Clarendon Press; 1990.

3.   Eberhart M. A quantum description of the chemical bond. Philos Mag B. 2001;81(8):721–9.

4.   Jones TE, Eberhart M. The Bond Bundle in Open Systems. Int J Quantum Chem. 2010;110:1500–5.

5.   Heidarzadeh, F.; Shahbazian, S., The Quantum Divided Basins: A New Class of Quantum Subsystems. Int. J. Quantum Chem. 2011, 111, 2788-2801.

6.   Heidar Zadeh, F.; Shahbazian, S., Toward a fuzzy atom view within the context of the quantum theory of atoms in molecules: quasi-atoms. Theor. Chem. Acc. 2011, 128, 175-181.

7.   Ayers PW, Jenkins S. An electron-preceding perspective on the deformation of materials. J Chem Phys. 2009;130(15).

8.   Jenkins S, Blancafort L, Kirk SR, Bearpark MJ. The response of the electronic structure to electronic excitation and double bond torsion in fulvene: a combined QTAIM, stress tensor and MO perspective. Phys Chem Chem Phys [Internet]. 2014;16(d):7115–26.

9.   Jones TE. Nucleophilic substitution: A charge density perspective. J Phys Chem A. 2012;116(16):4233–7.

10.   Morgenstern A, Eberhart M. Bond dissociation energies from the topology of the charge density using gradient bundle analysis. Phys Scr. 2016;91(2):23012.

11.   Morgenstern A, Morgenstern C, Miorelli J, Eberhart ME. The influence of zero-flux surface motion on chemical reactivity. Phys Chem Chem Phys. 2016;18:5638–46.

12.   Miller JE. Relative Critical Sets in Rn and Applications to Image Analysis. University of Norther Carolina; 1998.

13.   Smiley MF, Milnor J. Morse Theory. [Internet]. Vol. 71, The American Mathematical

Monthly. 1964. 936 p. Available from:
http://www.jstor.org/stable/2312441?origin=crossref

14. Jones TE, Eberhart ME, Imlay S, MacKey C. Bond Bundles and the Origins of Functionality. J Phys Chem A. 2011;115(45):12582–5.

15. Morgenstern A, Wilson T, Miorelli J, Jones T, Eberhart ME. In search of an intrinsic chemical bond. Comput Theor Chem [Internet]. 2015;1053:31–7. Available from: http://dx.doi.org/10.1016/j.comptc.2014.10.009

16. Bearpark MJ, Bernardi F, Olivucci M, Robb MA, Smith BR. Can fulvene S1 decay be controlled? A CASSCF study with MMVB dynamics. J Am Chem Soc. 1996;118(22):5254–60.

17. Bearpark MJ, Blancafort L, Paterson MJ. Mapping the intersection space of the ground and first excited states of fulvene. Mol Phys. 2006;104(5–7):1033–8.

18. Sicilia F, Bearpark MJ, Blancafort L, Robb MA. An analytical second-order description of the S 0 /S 1 intersection seam: Fulvene revisited. Theor Chem Acc. 2007;118(1):241–51.

19. ADF2016. SCM, Theoretical Chemistry, Vrije Universiteit, Amsterdam, The Netherlands, 2014.

20. SCM. ADF Manual. 2013;1–442.

21. Tecplot 2014 [Internet]. Available from: http://www.tecplot.com/

22. Bersuker I. The Jahn–Teller Effect [Internet]. Cambridge: Cambridge University Press; 2006 [cited 2017 Oct 20]. Available from: http://ebooks.cambridge.org/ref/id/CBO9780511524769

23. G. S. Hammond, Journal of the American Chemical Society 77, 334 (1955),

24. Berlin T (University of M. Binding Regions in Diatomic Molecules. J Chem Phys. 1951;19(2):208–13.

25. Wang W, Hobza P. Application of Berlin's Theorem to Bond-Length Changes in Isolated Molecules and Red- and Blue-Shifting H-Bonded Clusters. Collect Czechoslov Chem Commun [Internet]. 2008;73(6–7):862–72. Available from: http://cccc.uochb.cas.cz/73/6/0862/

26. Wang X, Peng Z. Binding regions in polyatomic molecules. Int J Quantum Chem. 1993;47(5):393–404.
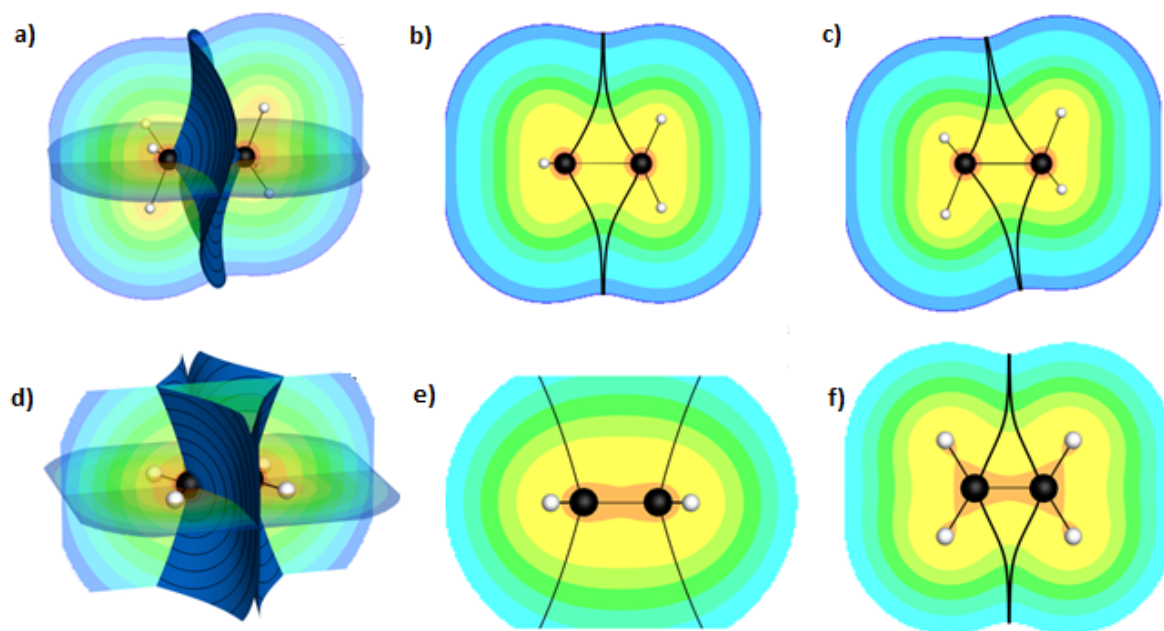
Figure 3: (a-c): The surfaces of the C-C bond bundle of ethane and two perpendicular cut planes containing the C-C axis. The BB converges in all directions as can be seen by the intersection of the bond bundle with the xz (b) and yz (c) cut plane. (d-f): The surfaces of the C-C bond bundle of ethane and two cut planes. The surfaces of this bond bundle are diverging perpendicular to the xz plane shown (e), and converging in the plane of the molecule (f). The bond bundle of ethene is said to be open normal to the molecular plane and closed in the plane.
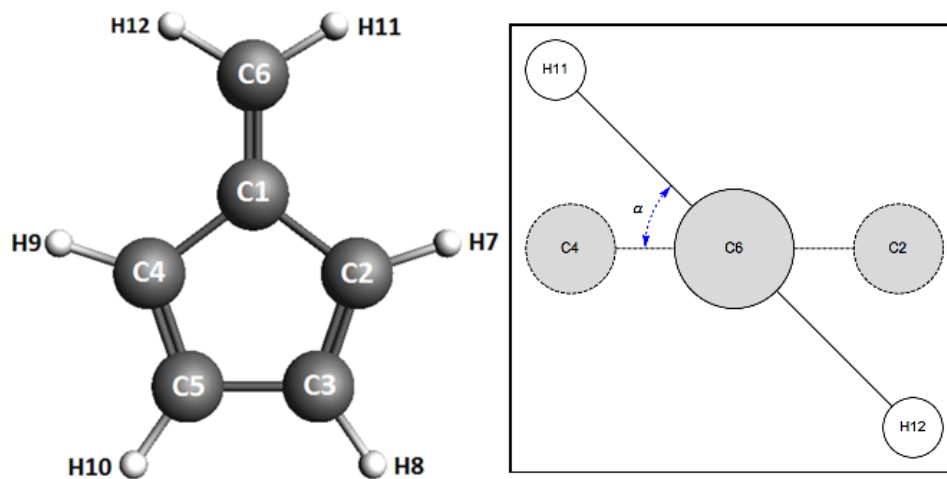
Figure 4: Fulvene molecule (left) with carbon (C1-C6) and hydrogen (H7-H12) atoms labeled. The rotation of the methyl group about the C1-C6 bond axis is depicted on the right. The methyl group is rotated in $\alpha=10°$ increments from planar to the ring ($0°$) to perpendicular to the ring ($90°$).
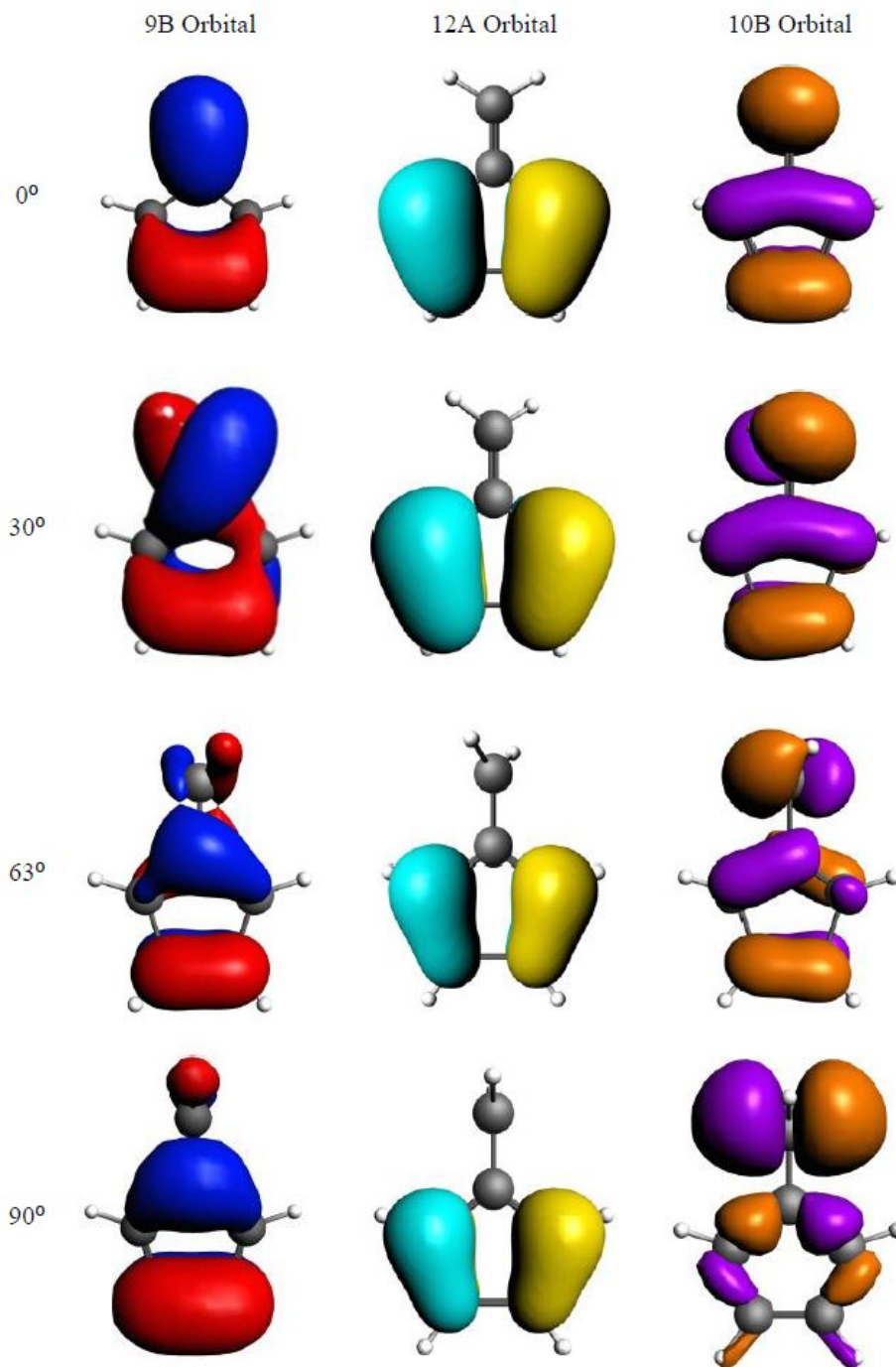
Figure 3: The near fermi energy SOs of the S_{63} coupled by the rotation (see Figure 4). The 9B SO is π-bonding between C1 and C6 while the 10B SO is π -antibonding between the same two atoms.
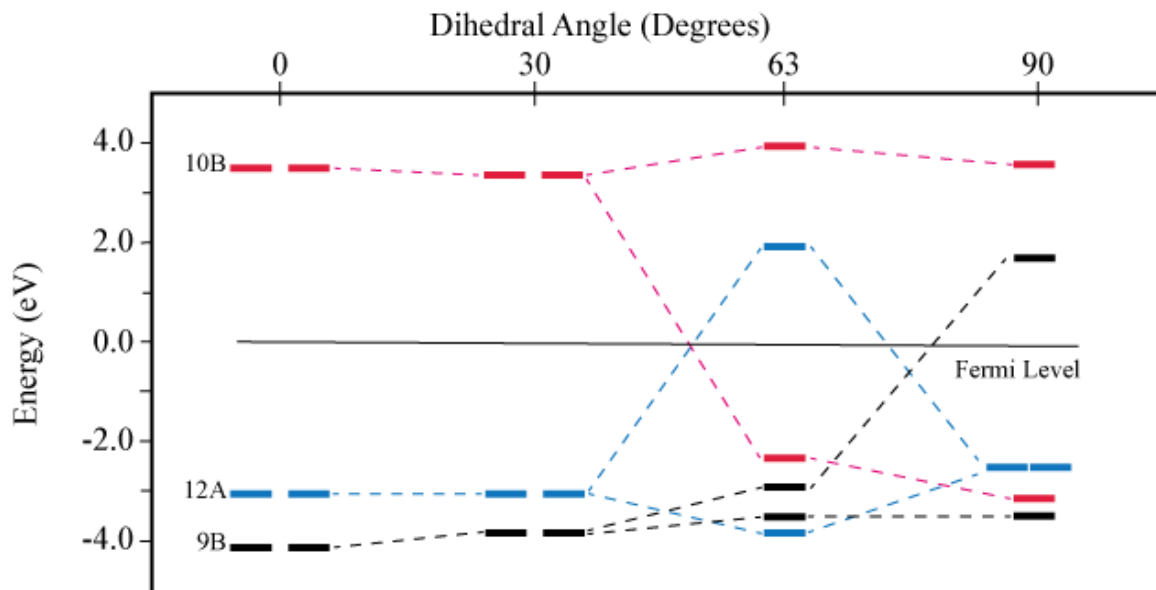
Figure 4: The SO levels diagram for O_1 at 0° and 30°, O_3 at 63°, and O_2 at 90° rotations.
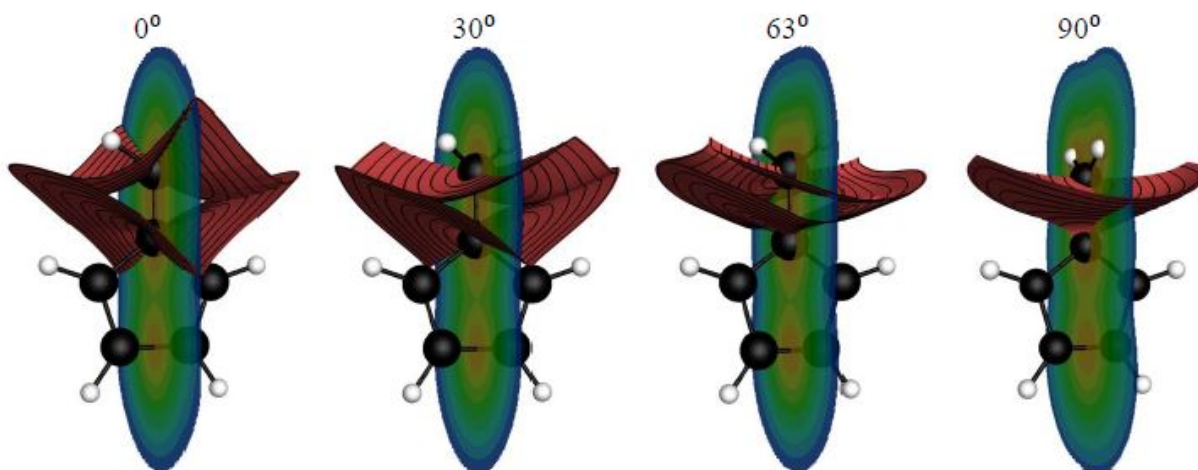
Figure 5: Fulvene C1-C6 bond bundles for O_1 as a function of rotation angle. The BBs for O_2 and O_3 show similar behavior, progressing from the open structure characteristic of ethene to the closed structure characteristic of ethane.
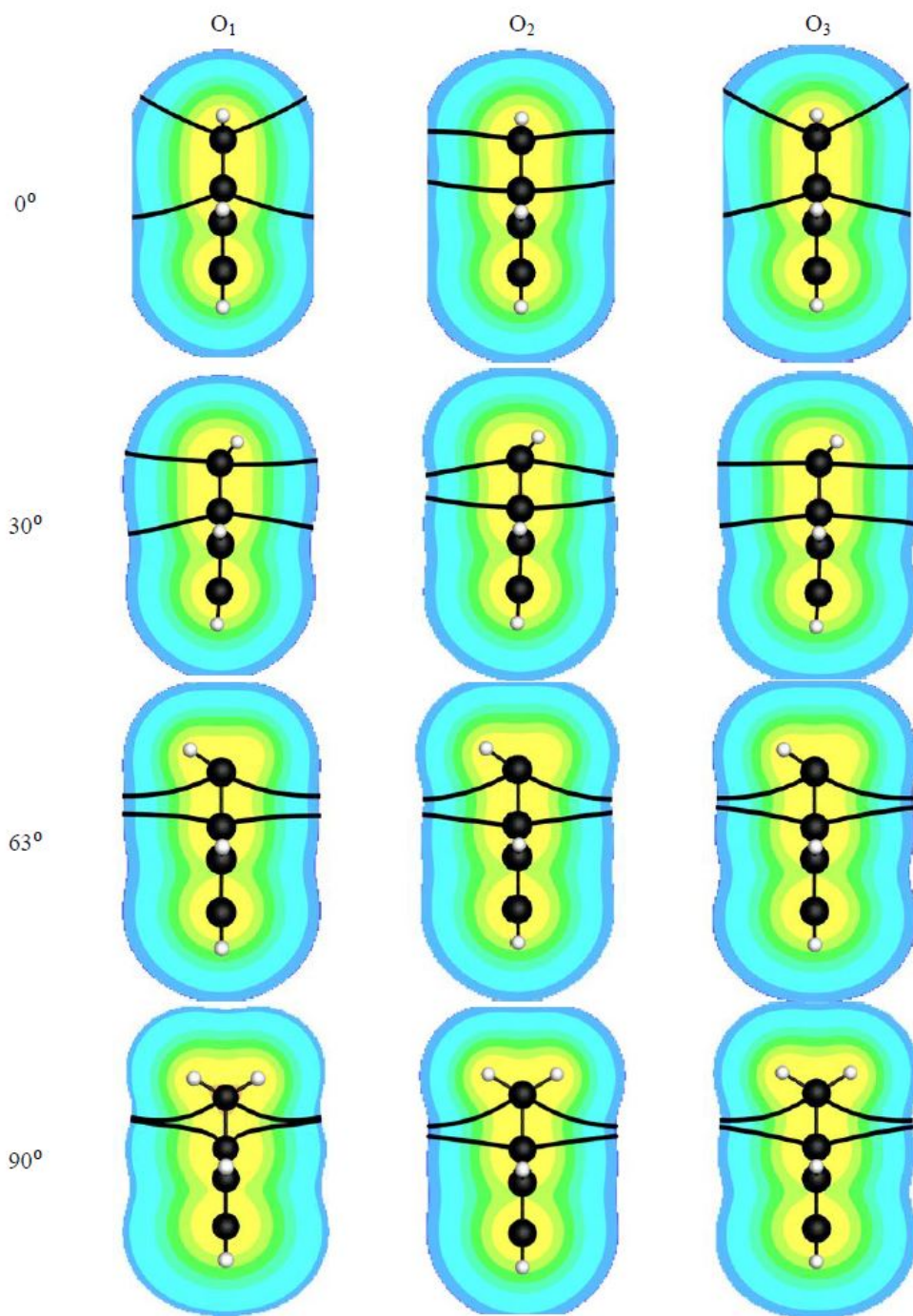
Figure 6: The heavy lines mark the intersection of the BB with the cut plane of Figure 5, permitting a more accurate assessment of BB closure for the three occupancies (columns) as a function of bond rotation (rows). Note the pronounced difference of the BB shapes for the three occupancies.
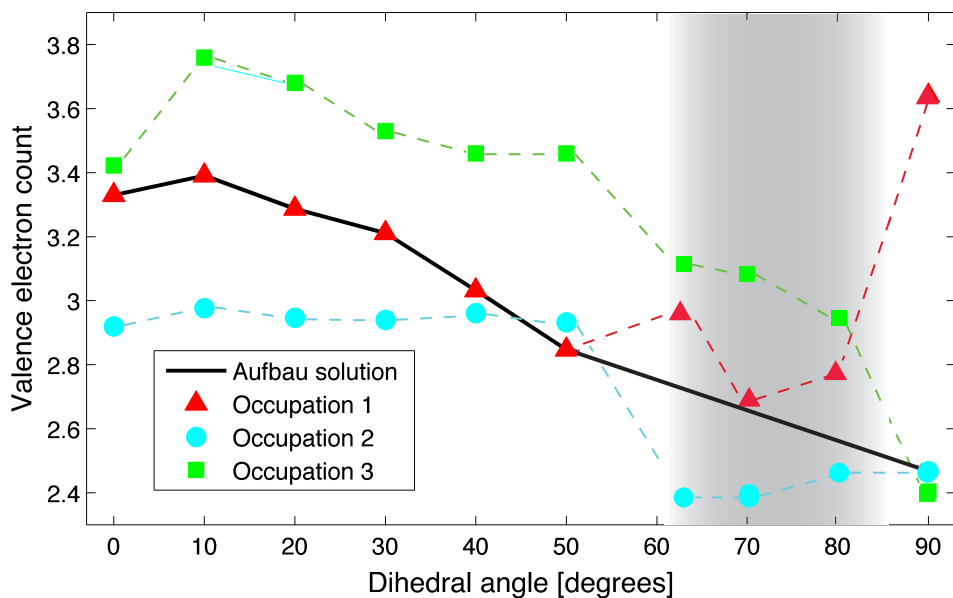
Figure 7: The valence electron count of the C1-C6 bond bundle for the full rotation of the methylene group on fulvene. The shade region corresponds to the points along the conical intersection where the nuclear and electronic wave-functions are inseparable. The black line connects the lowest energy occupancy with SOs occupied in accordance with the aufbau principle.

Evolution of Charge Density Attending Bond Torsion: A Bond Bundle Case Study Supplementary Information

Table S1: The C1-C6 bond length (pm) for 4 of the geometries discussed in the main text. The first row shows the bond length of the coordinates given by Jenkins, where the 30 degree rotations is that corresponding to a rigid rotation of the methylene group. The second through fourth row gives the ADF determined equilibrium C1-C6 bond length associated with the O_1, O_2 singlet and O_2 triplet configurations respectively. Note that for the appropriate occupancies, the CASSFC and MO DFT bond distances varied by at most 2%. Variation to the calculated BOs due to varying bond distances was determined through a sensitivity analysis. See Tables S2 and S3.

Degree Rotation	0 Deg C1-C6	30 Deg C1-C6	63 Deg C1-C6	90 Deg C1-C6
Coord. Provided by Jenkins	135	135	148	148
O_1 ADF Geometry	133	134	137	137
O_2 (singlet) ADF Geometry	142	144	146	145
O_2 (triplet) ADF Geometry	139	141	146	145

Sensitivity Analysis

During this study, we assessed the sensitivity of the bond bundle to changes in atomic coordinates, singlet versus triplet excited states, and functional. As an example, we computed the BB electron counts for an ADF relaxed geometry where the C1-C6 distance was held at 148 pm to the fully relaxed O_2 triplet geometry with a C1-C6 distance of 145 pm. The bond bundles are visually indistinguishable and the valence electron counts differ by 0.1 electrons, 3.46 and 3.56 valence electrons. In the same way, the choice of functional had no noticeable impact on the shape of the BBs and little quantitative influence, producing changes of less than 0.1 electrons. We take these observations as confirmation that the general trends associated with the bond rotation are captured by any reasonable density. Though this statement should not be taken to indicate that the quality of the density decomposed into BBs is irrelevant. Obviously, more accurate densities will provide more accurate decompositions and improved insight into charge density evolution.

Table S2: The bond lengths (in pm) for each geometry are shown.

Bond lengths (pm)													
Rotation °	0	10	20	30	40	50	63	63 B	70	70 B	80	80 B	90
C1-C6	135	134	134	134	135	135	136	148	138	145.3	139	146	148
C2-C1	147.9	147.1	147.1	147.1	147	146.8	146	140.9	146.3	140.2	145.8	140	142.4
C3 - C2	135.5	134.5	134.5	134.6	134.7	134.9	135.2	146.2	135.6	146.2	136	146.3	142.4
C4 - C1	147.9	147.1	147.1	147.1	147	146.8	145	140.9	146.3	140.2	145.8	140	142.4
C5-C4	135.5	134.5	134.5	134.6	134.7	134.9	136.2	146.2	135.6	146.2	136	146.3	142.4
C5-C3	148.3	147.2	147.1	147	146.8	146.5	146	137.1	145.8	135	145.4	135	141.3
H7 -C2	108	108	108	108	108	108	108	108	108	108	108	108	108
H8 -C3	108	108	108	108	108	108	108	108	108	108	108	108	108
H9 - C4	108	108	108	108	108	108	108	108	108	108	108	108	108
H10 -C5	108	108	108	108	108	108	108	108	108	108	108	108	108
H11-C6	108	108	108	108	108	108	108	108	109	108	109	108	108
H12-C6	108	108	108	108	108	108	108	108	109	108	109	108	108

Table S3: Selected properties for fulvene at incremented angles calculated during the study. The first column on the left shows the calculated O_1 valence electron count in the bond bundle and second column presents the O_1 bond bundle volume. The O_2 triplet and singlet valence electron counts and volumes are shown in the next 4 columns. Finally, the last 2 columns on the right show the C6-H11 valence electron count and bond bundle volume for the S_0 and S_{90} geometries.

Degree	O_1 Electron Count	O_1 BB Volume	O_2 (triplet) Electron Count	O_2 (triplet) BB Volume	O_2 (singlet) Electron Count	O_2 (singlet) BB Volume	O_2 C6-H11 Electron Count	O_2 C6-H11 BB Volume
10	3.391	74.650	-	-	-	-	-	-
20	3.287	70.760	-	-	-	-	-	-
30	3.211	68.330	3.184	48.840	-	-	-	-
40	3.032	62.850	-	-	-	-	-	-
50	2.847	57.950	-	-	-	-	-	-
63	2.357	48.610	3.109	48.509	2.370	36.810	-	-
70	2.676	53.410	2.748	44.578	-	-	-	-
80	2.781	55.270	2.707	44.120	-	-	-	-
90	3.640	66.678	2.468	44.900	2.256	36.076	2.299	72.46

Table S4: Bader analysis properties calculated by ADF referenced in the results section. For S_0 and S_{90} geometries the density, net charge, spin density, and Laplacian were calculated for each atom in fulvene. The last column on the right shows the change in net charge when you move from S_0 to S_{90} giving a better idea of the electron movement throughout the molecule during bond torsion.

Atom	S_0 Bader Analysis, O_1				S_{90} Bader Analysis, O_2				Δ Net Charge
	Density	Net Charge	Spin Density	Laplacian	Density	Net Charge	Spin Density	Laplacian	
C1	5.9987	0.0013	0	-1.17E-02	6.0101	-0.0101	0.4936	-1.42E-04	-0.4937
C2	6.0418	-0.0418	0	2.30E-04	6.0418	-0.0418	-0.0135	-1.69E-03	0.0118
C3	6.0300	-0.0300	0	-6.26E-03	6.0143	-0.0143	0.2775	-5.80E-03	-0.2833
C4	6.0418	-0.0418	0	2.30E-04	6.0418	-0.0418	-0.0135	-1.69E-03	0.0118
C5	6.0300	-0.0300	0	-6.26E-03	6.0143	-0.0143	0.2775	-5.80E-03	-0.2833
C6	6.0006	-0.0006	0	-6.04E-04	6.0612	-0.0612	0.8921	-7.92E-03	-0.9000
H7	0.9759	0.0241	0	2.45E-03	0.9798	0.0202	-0.0008	5.79E-04	0.0014
H8	0.9726	0.0274	0	4.91E-03	0.9712	0.0288	0.0047	4.95E-03	0.0002
H9	0.9759	0.0241	0	2.45E-03	0.9798	0.0202	-0.0008	5.79E-04	0.0014
H10	0.9726	0.0274	0	4.91E-03	0.9712	0.0288	0.0047	4.95E-03	0.0002
H11	0.9800	0.0200	0	4.52E-03	0.9572	0.0428	0.0393	5.57E-03	-0.0337
H12	0.9800	0.0200	0	4.52E-03	0.9572	0.0428	0.0393	5.57E-03	-0.0337
	--								
Total	41.999	0.0001	0.0000	-0.0006	41.999	0.0001	2.0001	-0.0008	0